Chapter 3

The detector: DØ

The DØ detector presently in operation at the DØ collision hall at Fermilab has been constructed to study $p\bar{p}$ collisions at $\sqrt{s} = 2$ TeV in the Tevatron collider. Figure 3.1 shows a cut-away view of the detector.

The prime focus of the DØ experiment is to study high mass states and large p_T phenomena. This includes the search for the top quark, critical tests of the standard electroweak theory through precision study of the W and Z bosons, various studies of perturbative QCD (PQCD), the production of b quark hadrons as well as searches for new phenomena beyond the "Standard Model". Such goals call for the features on which the detector has been optimized [47], namely, excellent identification and measurement of electrons, photons, muons and good measurement of parton jet momenta covering the full 4π solid angle and the resultant fine measurement of the missing transverse energy ($\vec{\not{E}}_T$) which is the signature of neutrinos and other non-interacting particles. The detector design that emerged from the negotiation between these ambitions and the obvious constraints on available resources featured

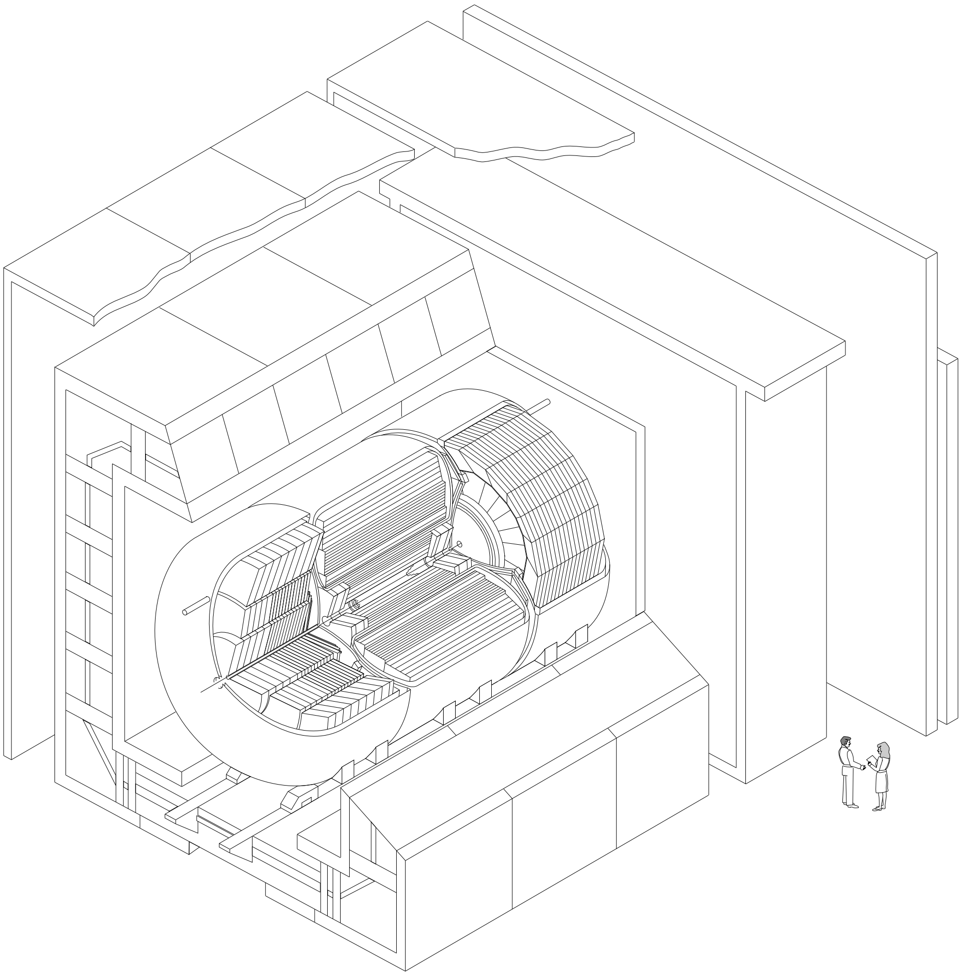

three major components:

Figure 3.1: A cutaway isometric view of the DØ detector.

• A compact non-magnetic central tracking system at the core. This system consists of four subdetectors and is known collectively as the Central Detector (CD). The CD traces the charged particle trajectories with adequate spatial resolution and also offers measurements of the absolute charge (using $\frac{dE}{dx}$ in drift chambers) and the absolute charge-to-mass ratio (using transition radiation) of the particles. These measurements are crucial in suppressing the backgrounds to electrons.

• A finely segmented thick sampling calorimeter that is hermetic, radiation-hard, compensating and stable over an extended period of time. The detector employs liquid argon (LAr) as the active material and uranium, stainless steel and copper plates as absorbers. The calorimeter forms the layer between the innermost CD and the outermost muon system. It is the heart of the DØ detector that provides accurate measurement of energy for photons, electrons and jets and the total transverse momenta of neutrinos and other non-interacting particles. It also offers confirmation for muons based on its trace of a minimum ionizing particle (MIP).

• A muon system with thick magnetized iron absorbers sandwiched between layers of proportional wire drift chambers. This allows momentum measurement for muons while keeping backgrounds from hadron punchthrough to a minimum.

All of the above components have a common denominator in that they rely on the production of charged particles in their sensitive volumes initiated by the particles of primary interest. Consequently, each component requires strong, well-controlled electric fields to drive these charged secondaries which carry all the available information about the primary to the readout channels in an orderly manner. It is thus of vital importance to develop and maintain a robust and reliable high-voltage system that keeps the detector alive.

Finally, all of these are of little use without a system that allows the experimenters to be in continuous communication with the detector. The huge amount of information coming out of more than 100000 channels at a tremendous rate requires an extremely sophisticated data acquisition system

(DAQ) to make efficient use of it. At DØ , this comprises of 3 levels of online triggers that sequentially sift out the most interesting events and store them for offline scrutiny.

In this chapter we will present a brief overview of some of these subsystems, a thorough understanding and proper functioning of which is essential for our analysis.

First, let us define the coordinate system we shall be using. Following the common practice, we use a right-handed cylindrical coordinate system to describe the events at DØ. The pole is at the nominal interaction vertex about which the detector is centered. The direction of the proton defines the polar axis (the z axis, $\theta = 0$). The azimuthal axis is horizontal such that $\phi = \pi/2$ points vertically upward. The center of mass (CM) of the partons involved in the hard-scattering is not necessarily at rest in the laboratory frame at a hadron collider. Only the z component of its boost is likely to be significant. This fact motivates the definition of "rapidity" of a parton:

$$y = \ln(\frac{E + p_z}{E - p_z}) \tag{3.1}$$

$\frac{d\sigma}{dy}$ is invariant under the Lorentz transformation for β_z. Conventionally, the "pseudorapidity" defined as

$$\eta \equiv -\ln{(\tan\frac{\theta}{2})} \tag{3.2}$$

is measured. For $M \ll E$, $\eta \approx y$. Vectors in the detector are usually defined by r,η and ϕ.

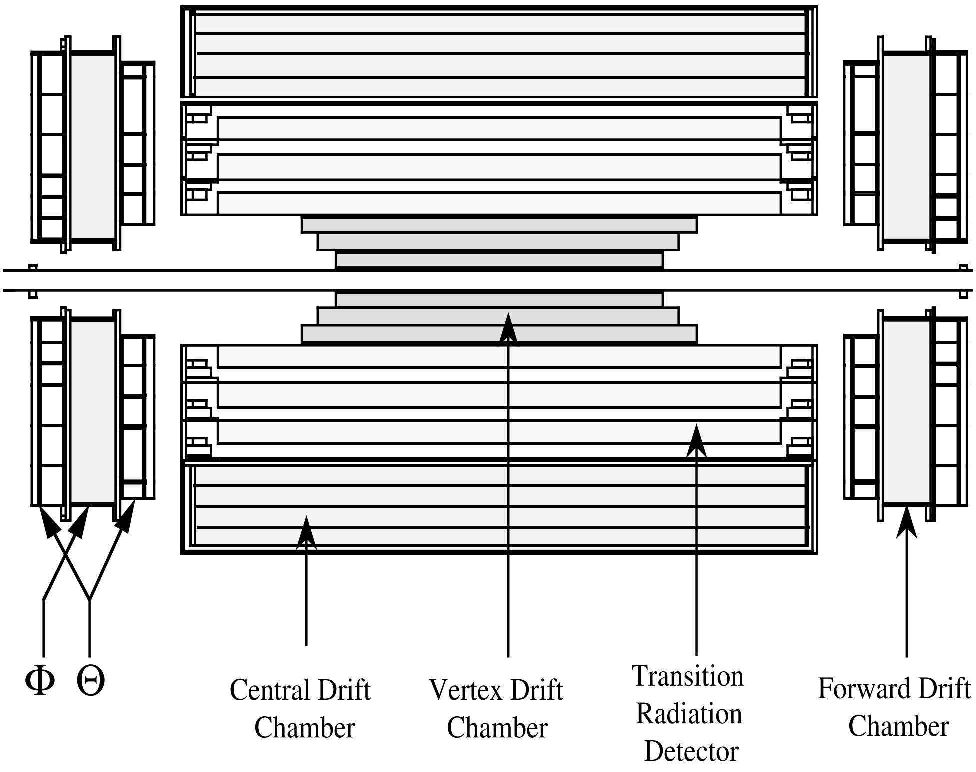

Figure 3.2: A side-view of the DØ central tracking system.

3.1 The central tracking system

A side-view of the the central tracking system at DØ , commonly known as the central detector (CD), is shown in Figure 3.2. It consists of four subdetectors. The lack of a magnetic field within the tracking volume has the obvious disadvantage of rendering the CD incapable of determining the momenta of the particles it tracks. However, it has some advantages too. A non-magnetic volume simplifies the job of tracking. For a given technology, it also allows a smaller volume: a consideration that becomes of critical importance as one moves outwards to the calorimeter and the muon systems where the size is a major limiting factor. Simpler technology and smaller size of the CD results in substantial savings in the overall cost of the detector.

3.1.1 Principle of operation of drift chambers

Three of the four subdetectors of the CD are drift chambers. The fourth employs drift chambers too, as one of its two components. We shall review the basic working principle of drift chambers before going on to describe each subdetector individually. A detailed account of the principle of operation of drift chambers can be found in References [48],[49]. In the gaseous medium of a drift chamber, an energetic charged particle causes ionization along its trajectory by Coulomb interactions. Sometimes the liberated electrons have sufficient energy to cause further ionization in the medium. Within statistical fluctuations in the macroscopic scale, the number of ion-pairs thus produced is proportional to the magnitude of the charge on the particle and independent of its energy in the highly relativistic limit. Particles such as the high-energy electrons that we are interested in cause sufficient ionization for detection at the cost of a negligible fraction of their total energy.

A well-controlled electrostatic field leads the swarm of electrons to drift towards an anode wire commonly known as a "sense wire" (SW). A multiwire drift chamber has several SWs strung parallel to each other forming a plane which usually divides the chamber in two symmetric halves. Consequently, this plane is often referred to as the "wire midplane". A detector typically has dozens of independent drift chambers, each called a "cell". The size of a cell is limited by the time-interval between successive bunch-crossings and the velocity of drift electrons in the gaseous medium. The electrostatic field in a cell divides its active volume into parts bearing a one-to-one correspondence with the SWs. Roughly speaking, an ionization electron finds its way to the sense wire closest to its site of creation. The small diameter of a SW (typically 20 μm - 50 μm) makes the field very strong in its immediate vicinity. This accelerates the drift electrons to energies high enough to cause further ionization in the medium leading to an avalanche multiplication. The signal amplification factor defined as the ratio between the number of electrons arriving at the SW to the number before the commencement of the avalanche effect is known as the "gas gain". Physical parameters are tuned to achieve a gas gain typically of a few tens of thousands which yields the optimal detection efficiency. The pulse formed by the electrons deposited on an SW are read out at one or both ends. A set of thicker field-shaping wires is usually strung between each pair of SWs to control the field near the latter and to reduce the coupling between them.

The velocity of the drift electrons is determined by the strength of the field and the composition, pressure and temperature of the medium with no dependence on the particle that initiated the process. The time spent by the pulse in traversing the path in the wire and the time between the collision and the initiation of the ionization process being negligible compared to the drift time, the difference between the known time of collision and the time of arrival of the signal at the readout gives the drift time. With a properly calibrated and monitored medium, this can be readily translated into a drift distance. The resolution is limited by the statistical fluctuations in the gaseous medium which are much higher compared to the denser solid state tracking devices. The solid state trackers are also faster and more compact.

Since the individual drift times do not tell which side of the midplane the electrons drifted from, each signal on a SW can be mapped onto two points on the plane perpendicular to it: one corresponding to the true track and the other to its mirror image. Thus arises the so-called question of "left-right ambiguity" for each segment (of a track) in a cell. This dilemma is easily resolved. A slight staggering of the SWs about the midplane breaks the symmetry between its two sides. Then the set of points corresponding to the segment of a true track, which is known to be a straight line in a non-magnetic volume, lends itself to a straight-line fit better than the set of mirror-images. If a track is built of multiple segments, a more powerful rejection of mirror images is achieved by the relative staggering of wire midplanes between cells in different layers (which contain the segments). Again, the idea is the same. A cut on the quality of the fit thus does a very good job of rejecting the mirror tracks with an excellent efficiency for the true tracks. This technique is applied in all the drift chambers at DØ whenever there is a left-right ambiguity to be dealt with.

The drift-distance information from a set of SWs forming a single midplane defines only the plane parallel to the individual SWs which contains the track (this plane is not necessarily parallel to the SW plane). By itself, this is not sufficient for the complete reconstruction of the track in three dimensions. One needs to fix another plane in order to solve for the track as the line of intersection between the two. Having another set of SWs forming a different midplane in a subsequent layer is one way of doing it. However, this would double the thickness of the tracking volume. Alternatives requiring

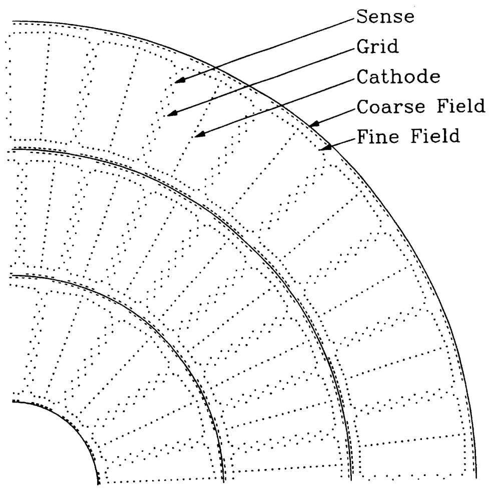

Figure 3.3: An end-view of one quadrant of the DØ vertex detector.

less additional volume are available and employed at DØ at the cost of some resolution. Each of the three tracking detectors at DØ has its own way of handling this which we will discuss individually. Finally, once the track is fully reconstructed in three dimensions, the amount of charge deposited on a sense wire, which is a measure of ionization per unit length of the charged particle track ($\frac{dE}{dx}$) can be used to determine the number of charge quanta associated with it.

A charged particle going through the "crack" of the boundary wall between two cells eludes either. To make up for this, it is often necessary to split the available depth into two or more layers of chambers with cell boundaries of subsequent layers staggered with respect to each other. The part of a track reconstructed by a cell is termed a "segment". This way, even if one segment is lost in a crack, a track can be built from those which are not.

Volume covered	r: 3.7 cm - 16.2 cm (in 3 layers of equal thickness) z: $\pm$48.5 cm (L0); $\pm$53.5 cm (L1); $\pm$58.5 cm (L2)
Cells	16 in Layer 0, 32 each in Layers 1 & 2
Sense wires (SW)	8 per cell; radial separation = 4.6 mm; stagger = 100 μm
Wire specifications	Anode: 25 μm NiCoTin; Field wires: 152 μm Au plated Al
Total channels	1280 (2 per SW)
SW voltage	+2.5 KV
Gas	CO_2 (0.95) + C_2H_6 (0.05) + H_2O (0.005) P = 1 atm; T = 25°C
Gas gain	$\sim 4 \times 10^4$
Mean drift field	$\sim$ 1 KV/cm
Mean drift velocity	$\sim$ 7.3 μm/ns
Resolution	$r\phi: \sim 60$ μm; $z: \sim 1.5$ cm

Table 3.1: Some important parameters for the DØ VTX.

3.1.2 The Vertex Chamber (VTX)

The innermost of the detectors, the VTX's main purpose is to determine the co-ordinates of the primary vertex (or vertices in case of multiple interactions). This knowledge is crucial for the calculation of the transverse energy of the objects detected by the calorimeter. It should be mentioned here that at DØ we do not rely exclusively on the VTX for this piece of information.

As shown in Figure 3.3, the VTX has 3 layers (numbered from 0 to 2) each supported by thin G10 bulkheads mounted on carbon fiber support tubes. Titanium tie rods connect each bulkhead to the next inner carbon fiber tube to support the wire tensions. The wire midplanes project onto the beamline

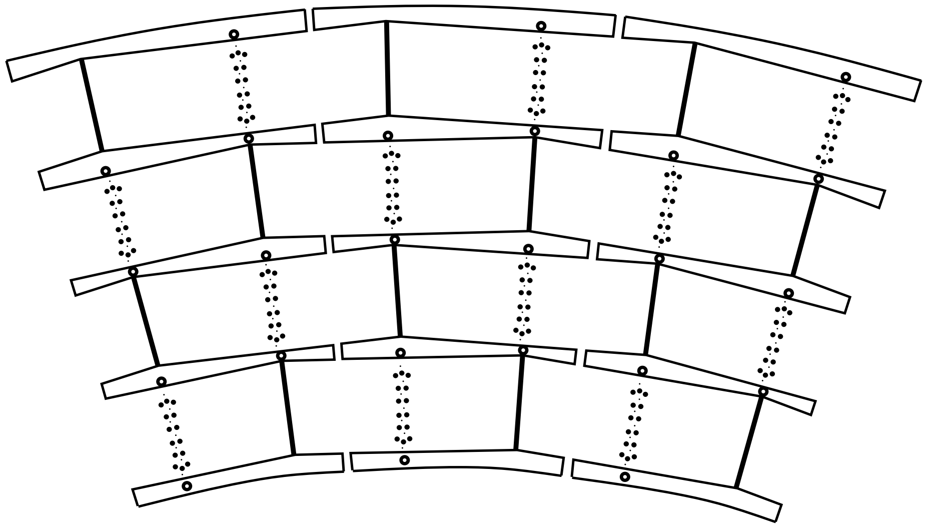

Figure 3.4: An end-view of one "3/32" of the DØ central drift chamber.

with the SWs, of which there are 8 per cell, running parallel to it. Drift distances are used to determine the coordinates of the vertex in the $r\phi$ plane. The resistive SWs are read out at both ends. The relative strength of the signals at the two ends is then translated into the z co-ordinate of the hit on a SW. This technique, known as "charge division", provides the supplementary information necessary for the complete reconstruction of a track in 3 dimensions. Some key numbers are summarized in Table 3.1 [50][51]. The very high flux density and limited space makes the reconstruction a difficult job in the VTX. Although the spatial resolution is quite good for a drift chamber, its efficiency for finding secondary vertices necessary for tagging b quark jets is rather poor.

3.1.3 The Central Drift Chamber (CDC)

The CDC performs the task of tracking in the Central volume of $| \eta |< 1.2$. It has a modular construction. 32 separate identical modules are assembled into a cylindrical shell, a part of which is shown in Figure 3.4. Each module is made from a Rohacell structure ("shelves" connected by "side-walls") covered with epoxy-laden Kevlar and coated with a double layer of 50 μm Kapton. Grooves are cut into each shelf to accommodate a Teflon tube containing the delay line (DL) where the wire midplane intersects the shelf. A field-shaping cage is printed with resistive ink on the Kapton surface with resistive ink. This cage, together with the anode wires (two between every pair of SWs) and the SWs themselves provide the desired field pattern inside the chamber. Each cell has 7 SWs parallel to the beam line with the wire midplane projecting onto it. The drift distance measurements are used for tracking in the $r\phi$ plane. The z coordinate is measured using the DLs of which there are two in each cell. A DL in the CDC consists of a coiled wire wound on a carbon fiber rod. A pulse on the nearest SW induces a signal on a DL. A higher gas gain (using higher voltage) and a grounded guard wire separates each outer SW (OSW) from the inner SWs (ISW) in an effort to minimize the possibility of an ISW inducing a signal on a DL. The signal induced on a DL propagates in either direction with a known velocity and is recorded at both ends. The time interval allows one to calculate the z-position of the inducing pulse. Thus, for a single track, there is a maximum of 28 points for a fit in the $r\phi$ plane and 8 in the rz plane. Some key numbers are listed in Table 3.2 [50][52][53][54].

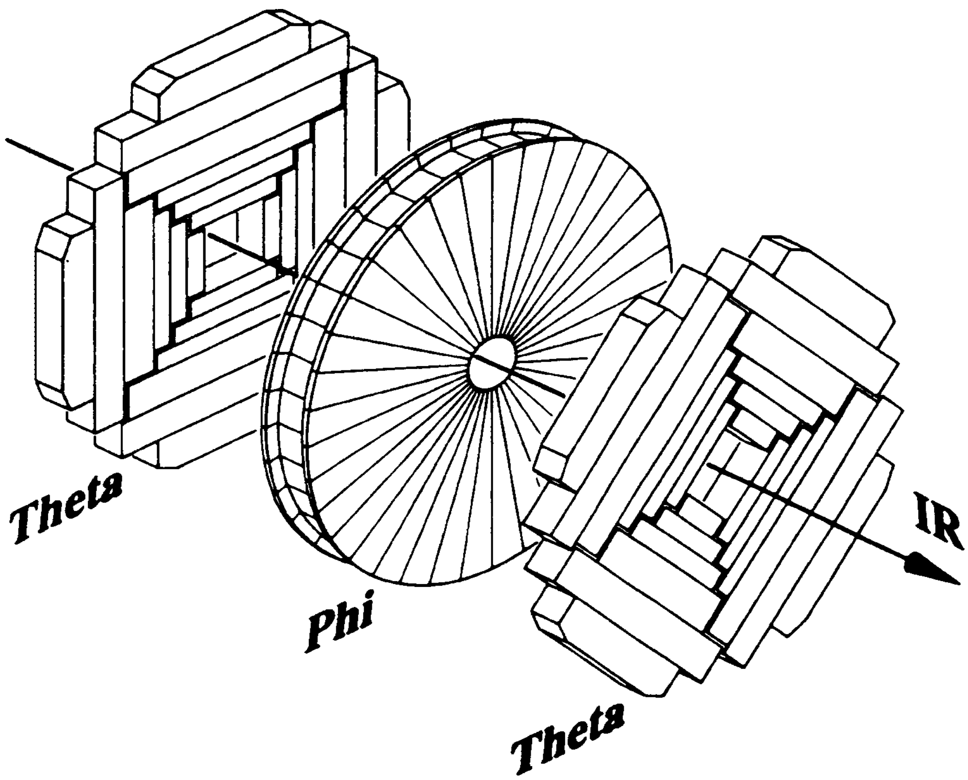

Figure 3.5: An exploded isometric view of one of the DØ forward drift chambers.

3.1.4 The Forward Drift Chambers (FDC)

As the name suggests, the purpose of the FDC is to perform tracking in the forward region which it does down to $|\eta| \approx 3.1$. One at each end, an FDC package consists of 3 modules: a Φ module sandwiched between a pair of Θ modules. Figure 3.5 shows an exploded isometric view of one FDC package. The Φ module performs tracking in the $r\phi$ plane and the Θ module, in the $r\theta$ plane. The FDC thus uses drift distances to construct two planes whose line of intersection gives the track. The materials used for construction are similar to those for the CDC. Each cell in a Φ module has 16 SWs strung radially with the wire midplanes projecting onto the beamline. A Θ module has four mechanically disjoint quadrants, each containing 6 cells. The length of a cell is proportional to its distance from the beamline. The 3 inner cells have the wire planes close to a wall. In these cells, there is no left-right ambiguity to be resolved. Each cell in a Θ module has 8 SWs and one delay line. For an event consisting of a single charged particle passing through the FDC, the two planes determined by the Φ and the Θ chambers would suffice for a complete 3D reconstruction of the track, rendering the delay line information superfluous. However, in the rather busy environment of the FDC in a typical hard-scattering process, there are often many tracks passing through a cell giving rise to many close combinations of planes. In such cases, the delay line provides a local measurement of ϕ to aid the correct matching of planes. Some key numbers are listed in Table 3.3 [50][55][56].

3.1.5 The Transition Radiation Detector (TRD)

When a charged particle crosses the boundary between two media with different dielectric or magnetic properties, photons are emitted in order to accommodate the abrupt change in the electromagnetic field. This phenomenon is known as "transition radiation" [57]. For highly relativistic particles ($\gamma > 10^3$), the radiation is primarily in the X-ray band, emitted strongly forward into a cone described by an angle $\alpha \propto \frac{1}{\gamma}$ with respect to the particle direction. An important feature of such radiation is that its intensity increases linearly with γ. The lightest of the charged hadrons, a pion is 275 times heavier than an electron. So, to produce transition radiation of the same intensity, ideally a charged pion would have to have 275 times the energy of an electron. At the Tevatron, electrons are the only charged particles likely to be produced with sufficient energy to induce detectable transition radiation. The DØ TRD is built to exploit this fact (however, let us not forget that nothing is ideal in the real world where separation of signal and background using the TRD proves to be a little more complicated than this might lead one to imagine).

For us, the most serious background to electrons comes from the electromagnetic jet produced by an energetic π^0 (decaying to $\gamma\gamma$) which has an associated track due to an overlapping low-energy charged particle. A magnetic field in the tracking volume would provide an excellent handle for the suppression of this background. In a detector like DØ , which has no magnetic field in its central tracking system, the measurement of transition radiation intensity can be used as a viable alternative.

One interface between two media of different dielectric constants does not suffice for reliable signal detection. Practical detectors are made up of stacks of thin foils, thereby providing many interfaces. The DØ TRD occupies the annular region between the VTX and the CDC. and is likewise cylindrically symmetric with respect to the beam-line [47][58]. It has three layers, each employing a "radiator stack" comprised of 393 layers of 18 μm thick polyethylene foil with a mean separation of 150 μm in a volume filled with nitrogen gas. Following each radiator stack radially outward, there is a two-stage drift chamber to accomplish the detection of the X-rays. Photoelectric absorption of the X-rays results in ionization of the gaseous medium producing a swarm of electrons mainly in the 15 mm first ("conversion") stage of the chamber. The charged primary also causes some direct ionization by Coulomb interactions. These electrons drift radially outward to the 8 mm second ("amplification and detection") stage of sense cells where the avalanche occurs. Xenon is employed as the drift gas because of its small attenuation length for X-rays. The 2 m long TRD has a pseudorapidity coverage of $-1.0 < \eta < 1.0$. 256 sectors covering the full azimuth give the TRD a fine segmentation in ϕ. In principle, the z-coordinate of a hit can be determined from the helical cathode pads, but this has not yet been achieved in practice. This limits its utility to relatively clean events only. Its signal rapidly loses meaning as the activity in an event in addition to the electron candidate to be tagged increases. A likelihood analysis of the TRD signal offers a rejection factor of 50 against pions with an efficiency of 0.90 for the electrons under the test-beam conditions.

3.2 The calorimeter

We shall first discuss the principles of operation of the DØ calorimeter briefly and then give some details of the apparatus.

3.2.1 Principles of sampling calorimetry

The purpose of a calorimeter is to measure energy. In particle detectors, this means measuring the energies of various particles. In the suitably chosen medium of a calorimeter, a particle is made to pass through so much material that it comes to rest after transferring all of its energy to the medium. This energy goes into the production of secondary particles. Some of the secondaries may be energetic enough to produce tertiaries and so on. The cascade that ensues is called a "shower" which continues to develop until a final state is reached where all the particles have energies below the threshold required for the production of a further generation. By studying the distribution of charged particles in the fully developed shower, one can classify it as either an electromagnetic or a hadronic shower with good confidence and also estimate its energy.

In a "sampling calorimeter" such as the one at DØ , "absorber" plates made of some material of very high density are arranged to form layers alternating with layers of an "active" medium [59]. The layers usually form planes normal to the direction of the incident primary. The absorber plates help contain the shower in a manageable volume, but the part of a shower contained in the absorber volume cannot be read out. It is the live material that allows the study of charged particle distribution. The name "sampling calorimeter" owes its origin to the fact that only that fraction of the shower's total energy which is deposited in the active volume is sampled. Not surprisingly, this fraction is known as the "sampling fraction". The detector is calibrated by measuring the sampling fractions accurately at the test-beam facility.

Electromagnetic and hadronic showers have marked differences in their characteristics owing to the fundamental difference between the dominant physical processes underlying them [60]. At high energies the electromagnetic showers result predominantly from bremsstrahlung losses by electrons and pair production by photons passing through a material medium. On an average, the energy retained by an electron of incident energy E_0 after passing through a distance x in a medium is given by

$$\langle E(x) \rangle = E_0 e^{-\frac{x}{x_0}} \tag{3.3}$$

x_0 is known as the radiation length and is a characteristic of the medium given approximately by

$$x_0 \frac{A}{Z^2} \times 180 \ \mathrm{gcm}^{-2} \tag{3.4}$$

where Z is the number of protons and A, the number of nucleons in the nuclei of the medium. DØ uses an electromagnetic calorimeter that is $20.5x_0$ thick in order to ensure that no electron would carry a significant fraction of its incident energy beyond it. The bremsstrahlung cross-section is inversely proportional to the square of the mass of the incident particle and increases logarithmically with the square of its Lorentz γ factor. At the Tevatron energies, any charged particle other than the electron is too heavy to lose a significant fraction of its energy by direct bremsstrahlung in the electromagnetic section (or in any other section) of the calorimeter. Charged particles also deposit some energy by ionization in the medium. For electrons, this effect dominates only below 100 MeV. Muons, which lose very little energy by bremsstrahlung, however do leave a trail of ionization in the calorimeter. Such a trace associated with a so-called "minimum ionizing particle" (MIP) plays a decisive role in the identification of muons at DØ .

In the following discussion, we shall use the terms "electron" and "positron" interchangeably. Our model assumes that at the energies of our interest, the sign of the charge is of no consequence; what is said of electrons applies to equally to positrons and this model does indeed work very well. Above ~ 100 MeV, electrons lose energy almost entirely by bremsstrahlung. For photons with energy greater than ~ 100 MeV, the dominant process is production of an e^+e^- pair. These two processes keep repeating alternately until all the final state particles are below ~ 100 MeV. In either case, the final state particles have an opening angle that is relatively small. This means that electromagnetic showers (which can be initiated either by an electron or by a photon) tend to be rather narrow compared to hadronic showers which we'll discuss next. Below 100 MeV, electrons lose energy primarily by ionization and photons by photoelectric absorption or Compton scattering. The expected number of charged particles in the shower is proportional to the energy of the initial electron or photon.

The development of a hadronic shower in matter is quite a bit more complex than that of an electromagnetic shower, making in unamenable to analytic treatment which makes it less well understood [61]. A high-energy hadron incident on a block of material eventually interacts with a nucleus of the medium via strong interaction. A generation of strongly interacting particles is thus produced to which the largest fraction of the incident hadron's energy is transferred on an average. A typical secondary hadron is produced with a transverse momentum of 350 MeV, so that hadronic showers tend to be more spread out both laterally and longitudinally than electromagnetic showers. A large portion goes into the production of π^0s (a π^0 decays promptly into two photons) and photons that initiate localized electromagnetic subshowers within the hadronic shower. The charged secondary hadrons cause ionization in the medium creating electric charge, the only quantity that the device can read. However, typically a third of the incident hadron's energy goes into processes that leave little or no signature in the calorimeter. These include the binding energy needed to break up the nuclei and the energy carried off by neutrinos and muons. Sometimes long-lived neutral hadrons like neutrons and K_L^0s can also escape undetected. The fraction of unseen energy has a much larger fluctuation in hadronic showers than in electromagnetic showers rendering the resolution of the former's energy proportionately poorer. The longitudinal and lateral development of hadronic showers scale with the nuclear interaction length defined as

$$\lambda \approx \frac{Z}{A\sigma_{\mathrm{abs}}} \tag{3.5}$$

where σ_{abs} is the cross-section for the nucleus-hadron inelastic collision. The relation

$$\frac{\lambda}{x_0} = 0.12Z^{\frac{4}{3}} \tag{3.6}$$

holds for high-Z materials, indicating that the higher the Z of the material, the easier it is to distinguish between electromagnetic and hadronic showers on the basis of their profiles. There are other criteria that dictate the choice of the live and the absorber materials in a calorimeter. One desirable feature is that the calorimeter's response to a shower should be independent of the size of its electromagnetic component at all energies, i.e. if e is the calorimeter's response to an electron and h that to a hadron (eg. $\pi^{\pm}$), both of energy E, then one would like to have $\langle e/h \rangle = 1$ for any E. A calorimeter with this feature is called "compensating". The choice of uranium as the absorber and liquid argon

(LAr) makes the DØ calorimeter nearly compensating with $\langle e/h \rangle = 1.11$ at 10 GeV falling to $\langle e/h \rangle = 1.04$ at 150 GeV. In some sections, stainless steel (SS) or copper (Cu) is used as the absorber. The very high Z of uranium helps make the detector compact and offers good hadron rejection from electromagnetic showers. Use of LAr also makes the calorimeter "unit gain", i.e. one in which no amplification (by avalanche multiplication) is needed for the detection of the charged secondaries. This makes the calorimeter stable over time: a single round of calibration before the first online commissioning can be expected to suffice for the entire life of the detector. One disadvantage and a major technical challenge is that the whole calorimeter must be kept in a cryostat to maintain the low temperature. A few words about energy resolution is in order before we review the DØ calorimeter briefly in the next section. The resolution of a sampling calorimeter can be expressed as follows [62]:

$$\left(\frac{\sigma_E}{E}\right)^2 = C^2 + \frac{S^2}{E} + \frac{N^2}{E^2} \tag{3.7}$$

where E is the energy of the incident particle and σ_E its resolution. The first of the three terms on the right hand side corresponds to the constant errors due to miscalibration such as fluctuations in the energy of the test-beam, the thickness of the LAr gaps etc. The second and the most important term is due to the sampling fluctuations. This is purely statistical in nature and can be justified by a naive treatment: Since the number of ions produced (N_{ion}) is expected to be proportional to E,

$$\langle N_{\text{ion}} \rangle = \alpha E \tag{3.8}$$

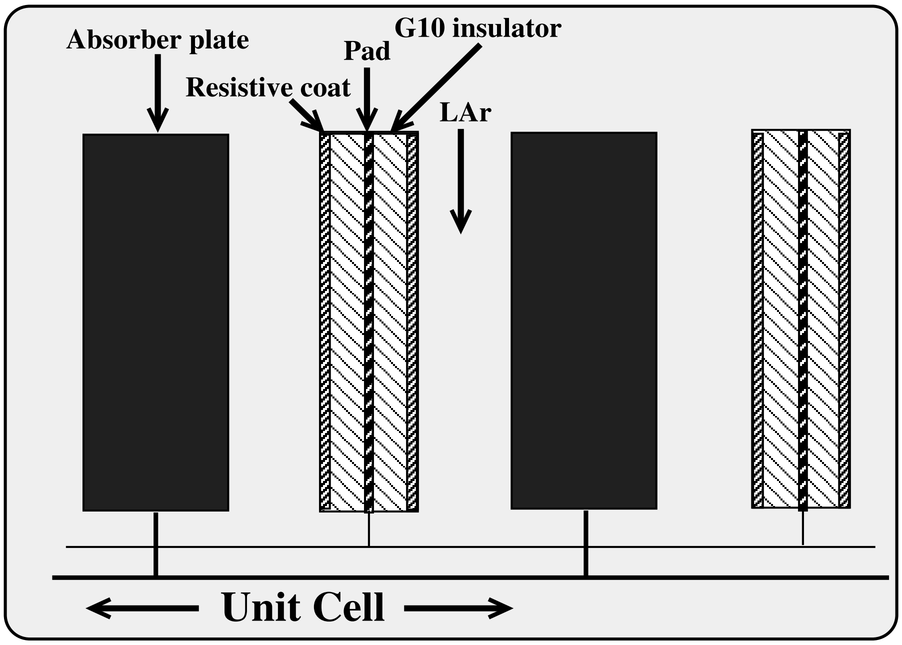

Figure 3.6: A schematic view of a unit cell of the DØ sampling calorimeter

and the detected signal D is proportional to $N_{\rm ion}$,

$$D = \beta N_{\rm ion} \tag{3.9}$$

therefore, applying Gaussian approximation to the Poisson distribution of $N_{\rm ion}$ ($N_{\rm ion}$ is large enough to justify this approximation) we get

$$\frac{\sigma(D)}{\langle D\rangle} = \langle N_{\rm ion}\rangle^{-1/2} = \alpha^{-1/2}\langle E\rangle^{-1/2}. \tag{3.10}$$

The last term arises from the noises such as electronic noise and the noise induced by the radioactivity of the absorber.

3.2.2 The apparatus

Figure 3.6 gives a schematic view (not to scale) of a single cell of the DØ calorimeter [47]. The thickness of an absorber plate varies between 3 mm and 46.5 mm depending on the module. LAr fills the gap of 2.3 mm between two adjacent absorber plates. A signal board is placed in the gap. The signal board consists of a copper readout pad sandwiched between two layers of G10 with a resistive layer of epoxy coating on their outer surfaces [63]. The epoxy is maintained at a positive potential with the copper plates at ground, the typical field strength being 8.7 KV/cm. The charge collected by the epoxy induces a signal on the readout pad. As opposed to a drift chamber or a scintillator, no amplification of the signal takes place in the medium itself, so the signal can be quite small. Thus, several cells are ganged together to increase the signal size and reduce the number of electronic channels. To allow access to the CD enclosed by the calorimeter, DØ has its main calorimeter system divided in 3 parts: one central and two endcaps, each submersed in a separate double-walled stainless steel cryostat. The central calorimeter (CC) provides coverage for roughly $|\eta| < 1$. Two endcap calorimeters (EC), each a mirror image of the other, extend the coverage to $|\eta| = 4$. There are also devices to plug some cracks that remain between the main systems. The calorimeters are modular in construction with a rather complicated geometry, but the general features are described below.

To best exploit the differences between the developments of electromagnetic and hadronic showers within the physical constraints, the modules are divided into three distinct classes: electromagnetic (EM), fine hadronic (FH) and coarse hadronic (CH). The names and locations of the various calorimeter module types at DØ are shown in Figure 3.7 which is a magnification of Fig-

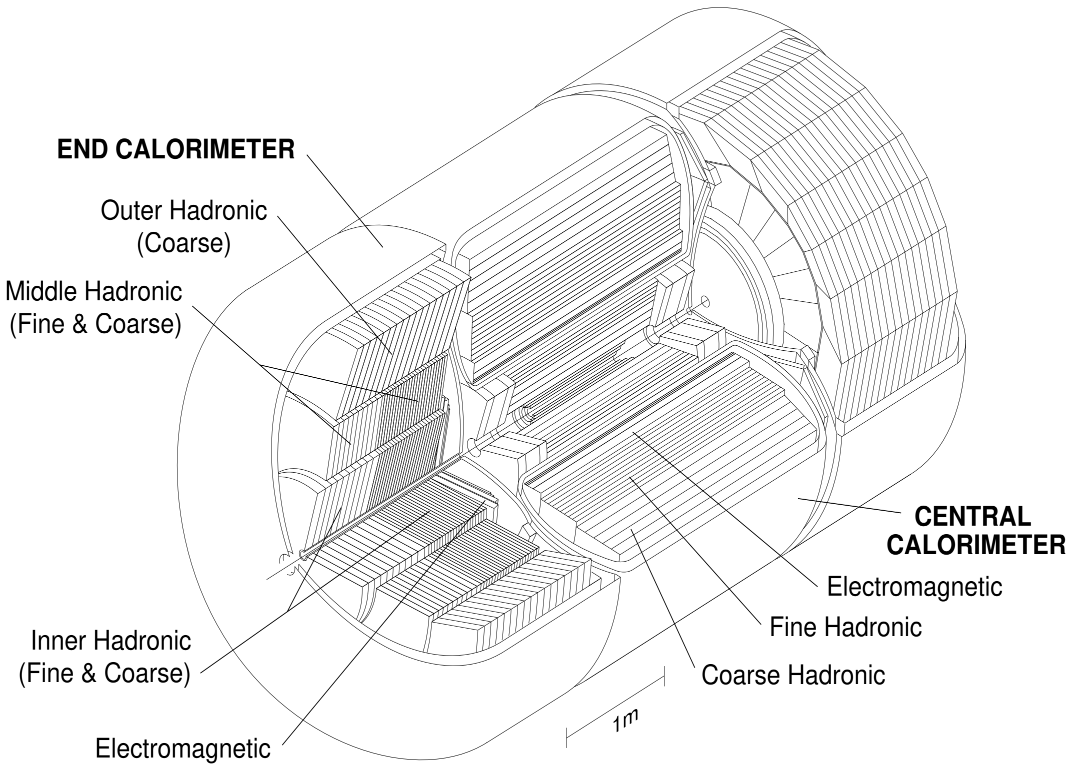

Figure 3.7: A cut-away view of the DØ calorimeter.

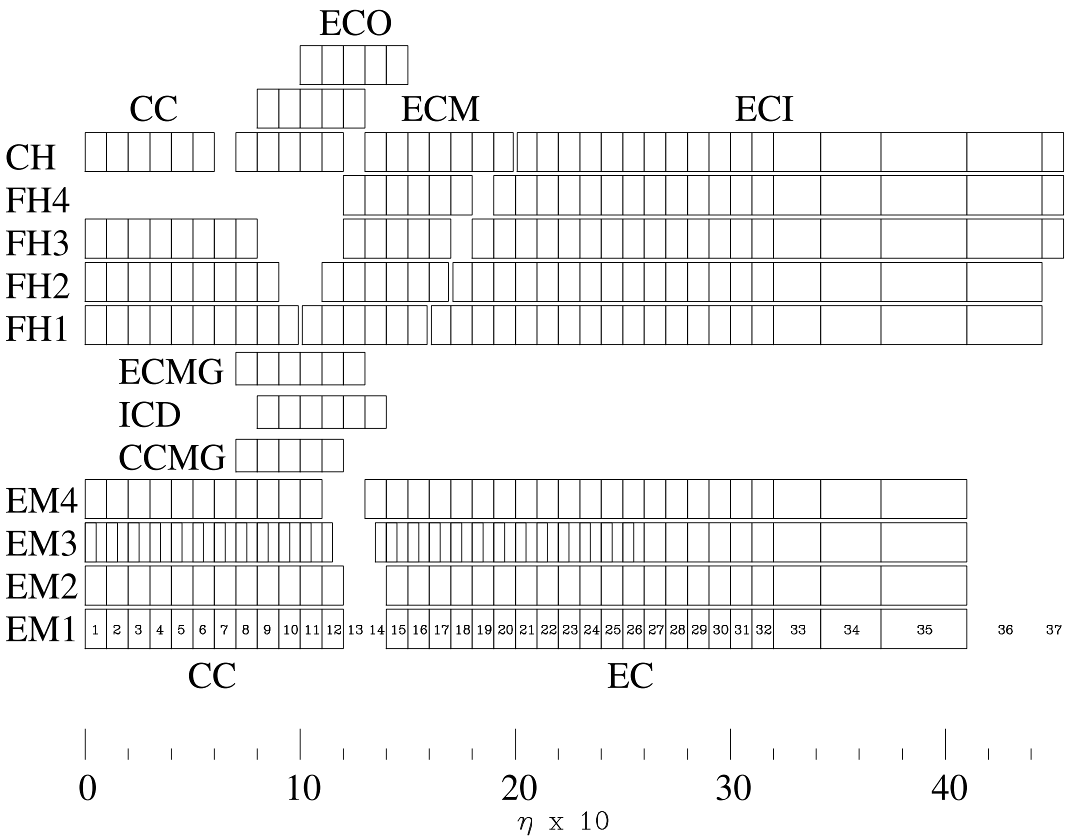

Figure 3.8: Projection of the DØ calorimeter on the $r\eta$ plane.

ure 3.1 without the muon system. The lateral and longitudinal segmentation of the DØ calorimeter is shown in Figure 3.8. The EM modules are closest to the nominal interaction point and are designed for full containment of electromagnetic showers. Their fine segmentation, longitudinally as well as laterally, is necessitated by the relatively short and narrow shape of electromagnetic showers. The EM modules have thin (3 to 4 mm) U plates. The FH modules have thicker U plates (6 mm). The bulk of a hadronic shower is expected to be contained within the EM and FH modules. The CH modules with their Cu (in CC) and SS (in EC) absorber plates are intended for the final containment of hadronic showers should any portion of it extend beyond the FH modules.

The lateral segmentation of the entire calorimeter is based on pseudoprojective towers. Most of the towers have a projective dimension of $\Delta\phi = 0.1$, $\Delta\eta = 0.1$. One exception is the third of the 4 layers in the EM section where an electromagnetic shower is expected to deposit most of its energy. Lateral segmentation in this layer is $\Delta\phi = 0.05$, $\Delta\eta = 0.05$. Fine segmentation such as this would be harder to implement using, for example, scintillator tiles or proportional wire chambers for the live volume. For large η, the spatial dimensions of $\Delta\eta = 0.1$ is rather small. Hence, in the high η region, some towers have a coverage of $\Delta\eta$ larger than 0.1. As a reference, a typical hadronic jet is expected to be contained within a cone of $\Delta R \equiv \sqrt{\Delta\phi^2 + \Delta\eta^2} \approx 0.7$.

There is a fair amount of uninstrumented material in the region of $0.8 <\mid \eta \mid< 1.4$ due to the cryostat walls and the support hardware. Two additional subsystems are employed to sample the showers in this region: the massless gaps (MG) and the intercryostat detectors (ICD). An MG has no absorber; it consists of a single readout board placed between the cryostat wall and the calorimeter modules. There are 160 readout channels per CCMG and 192 per ECMG. The ICDs are mounted outside the cryostats between the CC and each EC. They consist of plastic scintillator tiles with photomultipliers at the readout. The ICD tiles match the pseudoprojective structure of the rest of the calorimeter totalling 192 channels for each detector array.

Some parameters for the CC and the EC modules are shown in Tables 3.4 and 3.5 respectively [45]. The radiation and interaction lengths quoted apply to normal incidence. In the EC, the fine and coarse hadronic modules are grouped into middle (MFH, MCH) and inner (IFH, ICH) sections for readout purposes. There is also an additional outer hadronic (OH) section in the EC to plug a gap. The MCH and the OH readout channels are summed for $|\eta| > 1.4$. Thus, the table shows that these two module types share 64 channels.

The performance of the DØ calorimeters have been extensively studied at the test-beam facility. $C = 0.003 \pm 0.002$ and $S = 0.157 \pm 0.005\ \sqrt{\mathrm{GeV}}$ were obtained for electrons in the ECEM and $C = 0.032 \pm 0.004$ and $S = 0.41 \pm 0.04\ \sqrt{\mathrm{GeV}}$ for pions in the ECMH. The noise terms are negligible compared to these.

The position resolution is critical for electromagnetic jets since electrons are identified by matching a calorimeter cluster with a track in the CD. This resolution varies from 0.8 mm to 1.2 mm in the EM3 layer (shower maximum) over the full range of impact positions for 100 GeV electrons. The position resolution varies approximately as $E^{-1/2}$.

3.3 The muon system

Being too heavy for substantial bremsstrahlung and not participating in strong interactions, highly relativistic muons which are stable particles for the purpose of our detector, penetrate the calorimeter leaving only the trace of a minimum ionizing particle. In fact, other than the neutrinos, these are the only known particles capable of carrying a large transverse momentum past the calorimeter. They are measured in the muon detection system which forms the outermost layer of the DØ detector. The sideview of the entire DØ detector in Figure 3.9 highlights the muon system. The DØ muon detection system has five separate solid-iron toroidal magnets, namely three for the Wide An-

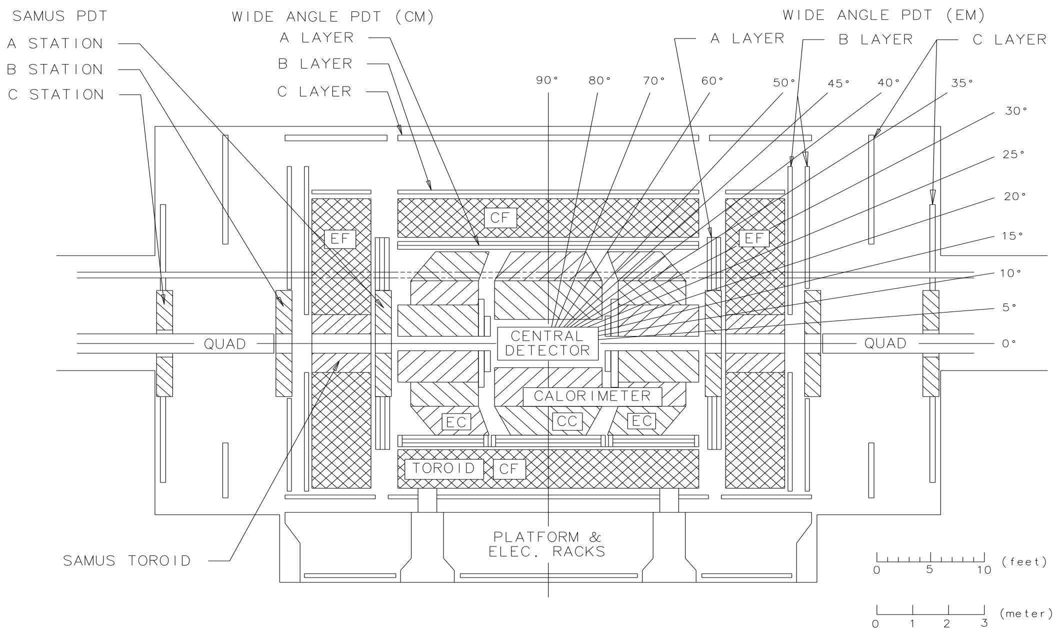

Figure 3.9: Elevation of the DØ detector.

gle MUon Spectrometer (WAMUS, one central iron (CF) and two end iron (EF) pieces) and two for the Small Angle MUon Spectrometer (SAMUS) [47]. Each of these magnets is sandwiched between layers of proportional drift tubes (PDT). The incident trajectory is determined from the interaction vertex and one layer (A) of PDTs that tracks the particle immediately before it enters the magnetic field of about 1.9 Tesla in the 1.7 m thick iron and two layers (B and C), separated by 1.7 m or more, track it after it has emerged from the field. The muon momentum is determined from the bend angle. The momentum resolution is limited mainly by multiple Coulomb scattering in the calorimeters and the iron. Each PDT has a rectangular cross-section and contains a single sense wire strung through its center. Several decks of PDTs make up a layer. The magnetic field bends the trajectory of a particle originating from

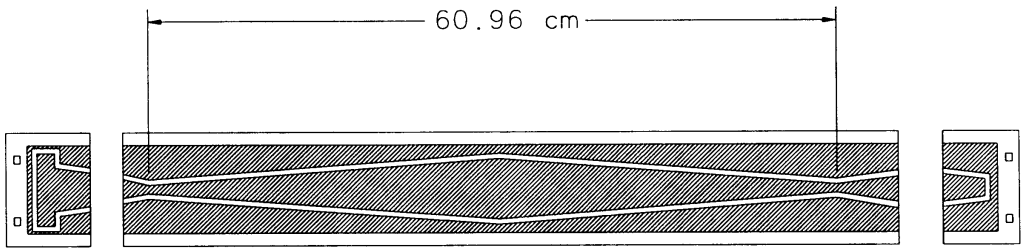

Figure 3.10: A WAMUS cathode pad.

the vertex mainly in the $r\eta$ plane. The sense wires run perpendicular to the beam direction so that the bend angle can be calculated from the accurate measurement of the drift distances. The time-to-distance map for the drift is fairly non-linear due to non-uniformity of the drift field. To map the track in the $r\phi$ plane, measurements of position have to be performed along the direction of the sense wires. This is done in two stages [64]. In the first stage, each sense wire is read out at both ends. The interval (Δt) between the times of arrival at the two ends provide a primary coarse measurement with a resolution of $\sim$ 10 cm. Each of the two walls of the PDT that are hit by a particle originating from the vertex have two cathode pads etched on them. The widths of the pads vary along the length in the shape of repeated diamond-like patterns with a wavelength of $\sim$ 61 cm as shown in Figure 3.10. A pulse on the sense wire induces one on each of the cathode pads. The widths of the cathode pads being a function of the position of the pulse on the sense wire along its length, so are the relative strengths of the induced pulses on the inner and the outer pads. Therefore, in the second stage, the measurements of the charge deposited on the cathode pads can be translated into the longitudinal position of the hit on the sense wire modulo the half-wavelength of the periodic pattern.

The Δt measurement performed in the first stage helps resolve this periodic ambiguity in the second stage where the resolution is about 3 mm. The muon system can measure the charged particle trajectories down to approximately 3° from the beam pipe.

Table 3.6 summarizes some of the important characteristics of the muon system.

3.4 The data acquisition system

The total cross section of $\overline{p}p \to X$ is approximately 70 mb ($= 7 \times 10^{-26}$ cm^2). At the typical luminosity of 5×10^{30} cm^{-2}s^{-1}, this translates into $\overline{p}p$ collisions at the rate of about 350 KHz. Only a very small fraction of these interactions are of interest to the experimenters. The DØ data acquisition (DAQ) system comprises of 3 levels of triggering to filter out the uninteresting events during online operation (i.e. these events are not recorded) and to perform a preliminary classification of the interesting events retained for offline analysis [47][65]. We shall briefly describe each of the levels individually before concluding this chapter. A simplified schematic diagram of the DØ DAQ is presented in Figure 3.11.

3.4.1 Level Ø (LØ)

LØ is a hardware trigger whose purpose is to tag the bunch-crossings which contain events that can be labeled "hard (or inelastic) scattering". To accomplish this, two hodoscopes in the forward regions are employed, one

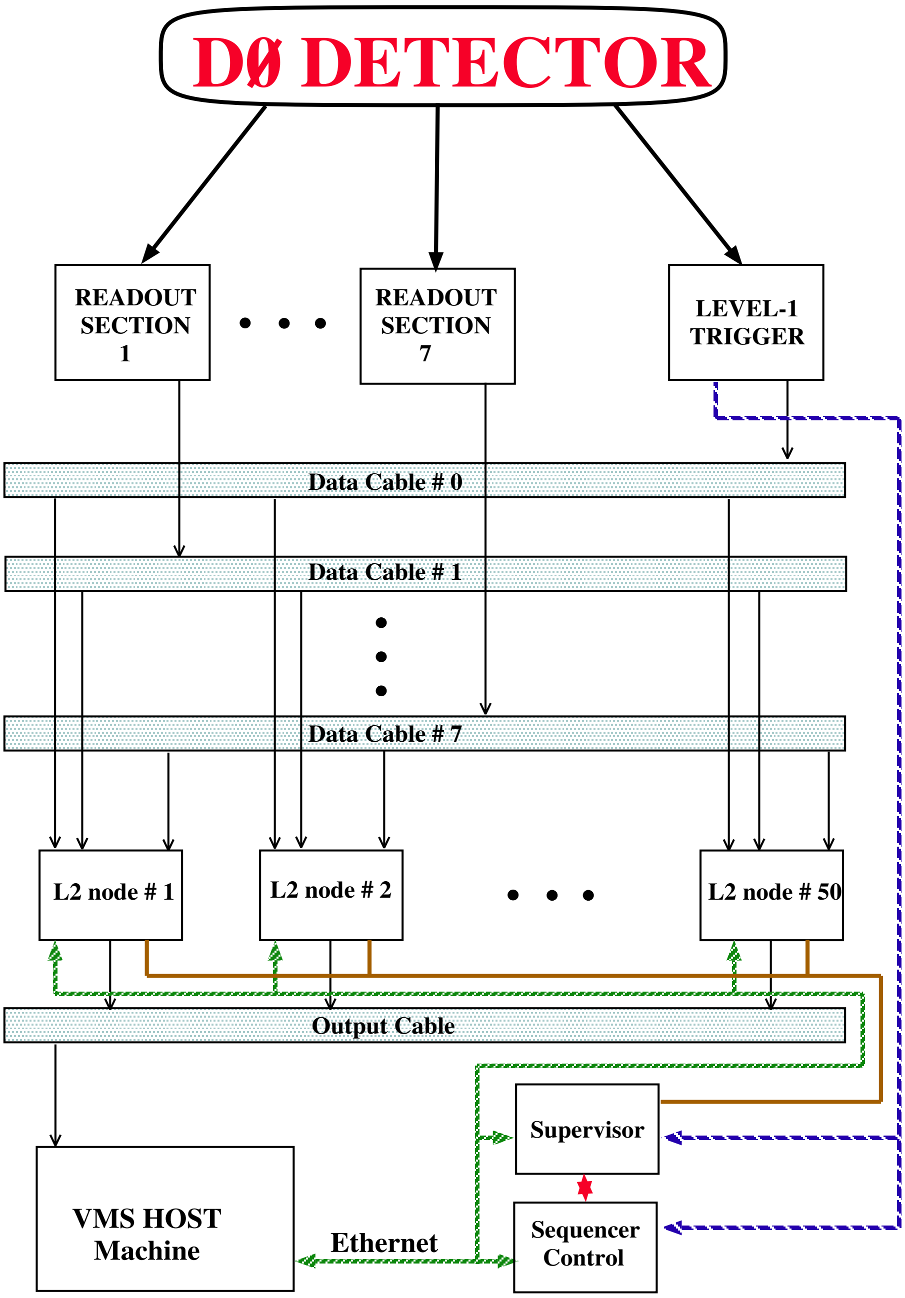

Figure 3.11: A schematic block-diagram of the DØ data acquisition system.

between each FDC and the neighboring EC cryostat [66],[67]. Each hodoscope consists of two arrays of rectangular scintillator tiles arranged at right angles to each other. Coverage in pseudo-rapidity is full between $2.3 <|\ \eta\ |< 3.9$. Due to the rectangular shape, only a partial coverage extends up to another 0.4 units in η on either side.

The LØ trigger registers the presence of an inelastic collision by detecting particles produced at low angles with respect to the beam. The probability of the requirement of coincidence between signals from the two hodoscopes being met by an inelastic collision exceeds 0.99. Timing information on the arrival of a signal at each array allows a crude determination of the z coordinate of a collision. A fast decision can be obtained within 800 ns of the beam-crossing with a resolution of 15 cm. A slower decision with a resolution of 3.5 cm takes about 2.1 μs. However, due to technical problems, this z information was not available for a part of run 1A.

3.4.2 Level 1 (L1)

L1 is another level of hardware triggers. A total of 32 triggers were available at L1 for run 1A. Each trigger is a logical combination of 256 programmable bits whose inputs come from LØ , the calorimeter and the muon system [68]. Since the L1 has only the 3.5 μs between two bunch crossing to make a decision, it can afford only the "fast z information" from LØ although for run 1A this provision was not enabled; only a fixed nominal value was used to calculate the transverse energies. The calorimeter trigger coverage extends to $\mid \eta \mid = 3.2$ in towers of 0.2×0.2 in the $\eta\phi$ space. Each "trigger tower" is further divided longitudinally into electromagnetic and hadronic sections. Thresholds on the E_T in the electromagnetic section of a trigger tower were used for various electromagnetic triggers (provisions for hadronic veto were available, but never used) while thresholds on the E_T in the entire tower (electromagnetic + hadronic) were used to tag jet candidates. Scalar and vector sum (for $\not{E}_T$) of the tower E_T's were also used for some triggers. For the muons, a loose requirement is made on aligned hits in the wire chambers. Hits are required in at least two layers within a 3-column ($\sim$ 60 cm) wide road in the WAMUS. Also used were some configurations of level 1 muon triggers which took several bunch-crossing intervals for decision. These are called level 1.5 triggers.

3.4.3 Level 2 (L2)

When an event is validated by L1, a complete digitization of the signals followed by a readout of the entire detector takes place. The event is then passed on to the L2 "software trigger system" for final filtering [69]. One member of the L2 computer farm consisting of 48 Microvax 4000-60's partially reconstructs and tests the event under a set of algorithms (also called "tool"s) for every L1 trigger satisfied. Specific tools for jets, electrons, photons, muons, $\not{E}_T$ and scalar E_T add up to a total of 128 [70].

The events passed by L2 proceed to the "host" computer system to be logged on tape under the template of "ALL stream". The maximum rate at which L2 could handle input events was about 200 Hz for run 1A. The pass rate into the ALL stream was limited to about 2 Hz. This rate is still too high for the offline reconstruction farm to keep up with in real time. A subset of the ALL stream events that passed some particularly stringent L2 tools are labeled "EXPRESS stream" to merit special special attention as the most interesting events. These events are immediately processed with the current reconstruction code and are recorded on separate tapes (these events are written on the ALL stream tapes as well). The pass rate into the EXPRESS stream is approximately 0.2 Hz.

3.5 Remarks

The overview presented in this chapter is only intended to provide the bare minimum of a groundwork deemed necessary for understanding the data analysis that follows. Several critical aspects such as the detailed organization of the data acquisition system, the high-voltage system, the monitoring and control systems, the clock etc have been completely omitted. Sufficient details of these systems are available in Reference [47].

Volume covered	r: 49.5 cm - 74.5 cm (in 4 layers of equal thickness); z: ± 90.0 cm
Cells	32 per layer
Sense wires (SW)	7 per cell; radial separation = 6.0 mm; stagger = 200 μm
Wire specifications Delay lines (DL)	Anode: 30 μm Au plated W; Cathode: 125 μm Au plated CuBe 2 per cell
DL velocity	2.35 mm/ns
Total channels	1408 (1 per SW, 2 per DL)
SW voltage	+1.45 KV (ISW); +1.58 KV (OSW)
Gas	Ar (0.93) + CH_4 (0.04) + CO_2 (0.03) + H_2O (0.005) $P = 1$ atm; $T = 25°$C
Gas gain	$\sim 2 \times 10^4$ (ISW); $\sim 6 \times 10^4$ (OSW)
Mean drift field	~ 620 V/cm
Mean drift velocity	~ 34 μm/ns
Resolution	$r\phi: \sim 180$ μm; $z: \sim 2.9$ mm
Tracking efficiency	0.89 (for isolated tracks)

Table 3.2: Some important parameters for the DØ CDC.

Chamber	Φ	Θ
Volume covered	r: 11.0 cm - 61.3 cm	11.0 cm - 62.0 cm (almost)
	$\mid z \mid$: 113.0 cm - 127.0 cm	104.8 cm - 111.2 cm (inner layer) 128.8 cm - 135.2 cm (outer layer)
Cells	36	6 per quadrant (4 quadrants per layer, 2 layers)
Sense wires (SW)	16 per cell	8 per cell
	separation = 8.0 mm; stagger = 200 μm	
Wire specifications	Anode: 30 μm Au plated W; Cathode: 163 μm Au plated Al	
Delay lines (DL)	None	1 per cell
DL velocity	-	2.35 mm/ns
Total channels	576 (1 per SW)	480 (1 per SW, 2 per DL)
SW voltage	+1.50 KV	+1.55 KV (ISW) +1.65 KV (OSW)
Gas	Ar (0.93) + CH_4 (0.04) + CO_2 (0.03) + H_2O (0.005) P = 1 atm; T = 25°C	
Gas gain	$\sim 3.6 \times 10^4$	$\sim 2.3 \times 10^4$ (ISW) $\sim 5.3 \times 10^4$ (OSW)
Mean drift field	$\sim$ 950 V/cm	$\sim$ 750 V/cm
Mean drift velocity	$\sim$ 37 μm/ns	$\sim$ 40 μm/ns
Resolution (drift)	$\sim$ 200 μm	$\sim$ 300 μm
Tracking efficiency	0.85 (for isolated tracks)	

Table 3.3: Some important parameters for the DØ FDC.

Calorimeter	EM	FH	CH
Number of modules	32	16	16
Absorber	U	UNb	Cu
Absorber thickness (mm)	3.0	6.0	46.5
LAr gap (mm)	2.3	2.3	2.3
Number of readout layers	4	3	1
Number of cells per layer	2,2,7,10	20,16,14	9
Total radiation lengths (x_0)	20.5	96.0	32.9
Total interaction lengths (λ)	0.76	3.23	3.17
Sampling fraction	0.1179	0.0679	0.0145
Total channels	10368	3000	1224
η coverage	± 1.2	± 1.0	± 0.6

Table 3.4: Some important parameters for the DØ Central Calorimeter.

Calorimeter	EM	IFH	ICH	MFH	MCH	OH
Number of modules	1	1	1	16	16	16
Absorber	U	UNb	SS	UNb	SS	SS
Absorber thickness (mm)	3.0	6.0	6.0	6.0	46.5	46.5
LAr gap (mm)	2.3	2.1	2.1	2.2	2.2	2.2
Number of readout layers	4	4	1	4	1	3
Number of cells per layer	2,2,6,8	4×16	14	4×15	12	3×8
Total radiation lengths (x_0)	20.5	121.8	32.8	115.5	37.9	65.1
Total interaction lengths (λ)	0.95	4.91	3.57	4.05	4.08	7.01
Sampling fraction	0.1190	0.0566	0.0153	0.0668	0.0164	0.0164
Total channels	7488	4288	928	1472	384+64+896	
$\mid \eta \mid$ coverage	1.3-3.7	1.6-4.45	2.0-4.45	1.0-1.7	1.3-1.9	0.7-1.4

Table 3.5: Some important parameters for the DØ Endcap Calorimeters.

Number of layers	3 (2 or 4 in some regions)
Number of decks per layer	4,3,3
Total number of modules	164
Total number of cells	11386
Interaction lengths (λ)	9.5 - 18.7
$\mid \eta \mid$ coverage	3.6
Drift gas	Ar (0.90) + CO_2 (0.05) + CF_4 (0.05) P = 1 atm; T = 25°C
Wire specifications	50 μm Au plated W; tension = 300g
High voltage	Anode (sense wires) : +4.56 KV Cathode pads: +2.3 KV
Max. drift distance	5.0 cm
Mean drift velocity	65 mm/μs
Resolution	drift distance: 0.2 mm position along the sense wire: 3 mm bend angle: 0.2 mrad momentum: $\delta p/p = ((0.18)^2 + (0.01 \cdot p)^2)^{\frac{1}{2}}$

Table 3.6: Some important parameters for the DØ muon detector.